Chemical Physics Impact 11 (2025) 100954

Contents lists available at ScienceDirect

Chemical Physics Impact

journal homepage: www.sciencedirect.com/journal/chemical-physics-impact

Full Length Article

Facile green synthesis of Co_3O_4 nanoparticles using *turmeric* extract: In vitro biomedical activities

Mais Mazin Al-Hamdani [a], Basima A.A. Saleem [b], Mohammed Ihsan Majeed [c], Mohamed Ahmed [d], Helal F. Hetta [e], Mohammed S. Saddik [a,f], Stefan Bräse [g,h,*], Mostafa F. Al-Hakkani [i,*]

[a] *Pharmaceutic Department, College of Pharmacy, Al-Ayen Iraqi University, AUIQ, An Nasiriyah, 64001, Iraq*
[b] *Department of Chemistry, College of Science, University of Mosul, Mosul, Iraq*
[c] *Pharmacy Department, Mosul Technical Medical Institute, Northern technical University, Iraq*
[d] *Dhofar University, College of Medicine, Oman*
[e] *Division of Microbiology, Immunology and Biotechnology, Department of Natural Products and Alternative Medicine, Faculty of Pharmacy, Universuty of Tabuk, Tabuk 71491, Saudi Arabia*
[f] *Department of Pharmaceutics and Clinical Pharmacy, Faculty of Pharmacy, Sohag University, 82524, Sohag, Egypt*
[g] *Institute of Biological and Chemical Systems- Functional Molecular Systems (IBCS-FMS), Karlsruhe Institute of Technology, Kaiserstraße 12, 76131, Karlsruhe, Germany*
[h] *Institute of Organic Chemistry (IOC), Karlsruhe Institute of Technology, Kaiserstraße 12, 76131, Karlsruhe, Germany*
[i] *Department of Methodology, MUP, Industrial zone, Arab El Awamer, Abnoub, 76, Assiut, Egypt*

ARTICLE INFO

Keywords:
Green chemistry
Cobalt oxide
Nanoparticles
Antibacterial
Anti-cancer

ABSTRACT

This research investigates the eco-friendly synthesis and comprehensive characterization of cobalt oxide nanoparticles (CoO—NPs) using turmeric ethanolic extract. Fourier transform infrared spectroscopy confirmed the presence of functional groups in the extract and their involvement in nanoparticle stabilization. Ultraviolet-visible spectroscopy revealed an absorption peak at 417 nm, with bandgap energies of 3.45 eV and 3.21 eV for direct and indirect transitions, respectively, as determined by Tauc's plot. X-ray diffraction analysis yielded an average crystallite size of 31.2 nm, while energy-dispersive X-ray spectroscopy verified the elemental composition. The nanoparticles displayed a zeta potential of -21.66 mV, and dynamic light scattering indicated a hydrodynamic diameter of 86.29 nm with a polydispersity index of 0.38. Transmission and scanning electron microscopy demonstrated an average particle size of 26.3 nm, featuring cubic structures and diverse surface morphologies. Antioxidant activity was evaluated using the DPPH assay, resulting in IC_{50} values of 3.82 mg/mL for the turmeric extract and 1.171 mg/mL for the CoO—NPs, compared to 0.42 mg/mL for BHT. The antibacterial efficacy of the CoO—NPs was assessed against Gram-positive *Bacillus subtilis* and Gram-negative *Escherichia coli*, with minimum inhibitory concentrations of 25.3 mg/L and 22.8 mg/L, respectively. Furthermore, the nanoparticles exhibited substantial anti-cancer effects, with IC_{50} values of 26.4 μg/mL against Caco-2 cells and 43.6 μg/mL against MCF-7 cells. This work advances green nanotechnology by integrating scientific innovation with environmental sustainability, thereby opening avenues for further research in materials science and biomedical applications.

Abbreviations: CoO-NPs, Cobalt oxide nanoparticles; MTT, Colorimetric assay for measuring cell metabolic activity; Caco-2 cell line, Colorectal carcinoma (ATCC: ATB-37); MCF-7 cell line, Breast cancer (ATCC: HTB-22); IC_{50}, Half maximal inhibitory concentration; ROS, Reactive oxygen species; HPLC, High performance liquid chromatography; DPPH, 2,2-diphenyl-1-picrylhydrazyl; BHT, Butylated hydroxytoluene; XRD, X-ray diffraction; ATR, Attenuated total reflection; FT-IR, Fourier-transform infrared spectroscopy; TEM, Transmission electron microscopy; SEM, Scanning electron microscopy; EDX, Energy dispersive X-ray; UV-Vis, Ultra violet spectroscopy; E_g, Energy band gap; MIC, Minimum inhibition concentration; *B. subtilis*, *Bacillus subtilis (ATCC 6633)*; *E. coli*, *Escherichia coli* (ATCC 8739).

* Corresponding authors.
E-mail addresses: mais.yahya@alayen.edu.iq (M.M. Al-Hamdani), basmasaleem@uomosul.edu.iq (B.A.A. Saleem), elmokhtarma@aun.edu.eg (M. Ahmed), hhussen@ut.edu.sa (H.F. Hetta), mohammed.sherif@pharm.sohag.edu.eg (M.S. Saddik), stefan.braese@kit.edu (S. Bräse), dr.mostafa.farouk.83@gmail.com (M.F. Al-Hakkani).

https://doi.org/10.1016/j.chphi.2025.100954
Received 9 May 2025; Received in revised form 14 October 2025; Accepted 18 October 2025
Available online 19 October 2025

1. Introduction

With rapid advancements in science, nanobiotechnology has emerged as an integrative field that combines technological innovation with environmental sustainability to benefit humanity [1]. The green synthesis of cobalt oxide nanoparticles (CoO—NPs) exemplifies a sustainable approach to nanomaterial production, as researchers seek to develop methods that balance technological efficacy, environmental responsibility, and economic viability [2]. Recent studies underscore the importance of CoO—NPs in various biomedical domains, particularly microbiology and therapeutics [3–5]. Advanced research has revealed their unique properties, including high efficacy and potential as safe alternatives to conventional treatments, such as antibacterial and antifungal agents [6,7]. Moreover, their application as anti-cancer agents opens new avenues in modern medicine and innovative therapies [8,9].

CoO—NPs play a crucial role in numerous applications, including catalysis in chemical processes [10], energy storage [11], and diverse biomedical applications [12–14]. These nanoparticles can be prepared using various chemical and physical methods, as well as environmentally friendly green methods [15]. Among the well-known chemical methods is the use of chemical precipitation reactions in aqueous solutions [16], where cobalt salts are mixed with a reducing agent in an aqueous solution, leading to the formation of cobalt oxide nanoparticles. Additionally, thermal decomposition methods can be employed [17], where cobalt compounds are heated in an oxygen-free environment at high temperatures to produce the nanoparticles, solution combustion [18,19], microwave-assisted [20,21], and co-precipitation [22]. As for physical methods, chemical or physical vapor deposition [23] can be utilized to produce CoO—NPs with controlled size, shape, and desired properties. In recent years, green methods have gained increasing attention, where plant extracts [24–26] or bacteria [24,27,28] can be used as reducing agents to produce cobalt oxide nanoparticles in an environmentally friendly manner [29–31]. These green methods are promising due to their scalability, reduced environmental pollution, and a wide variety of applications [32,33].

The present study adopts a multidisciplinary framework, integrating nanotechnology, biochemistry, and molecular biology. Emphasis is placed on the use of plant extracts as bioreducing agents, offering a sustainable alternative to traditional chemical techniques while mitigating adverse environmental effects. These extracts facilitate the eco-friendly production of nanoparticles through functional groups such as carbonyls, hydroxyls, primary amines, and polyphenols.

Turmeric and its derivative curcumin (diferuloylmethane) are rich in polyphenols and flavonoids. Studies have shown that turmeric contains approximately 6.3 % protein, 5.1 % fat (including essential fatty acids), 69.4 % carbohydrates, and vitamins such as riboflavin [34]. It exhibits diverse bioactive properties, particularly in biomedical contexts, exemplifying nature-derived sustainable resources. These include antioxidant, anti-inflammatory, anti-platelet aggregation, antimicrobial, antimutagenic, anti-cancer, and neuroprotective activities [35,36]. The composition of turmeric, encompassing polyphenols, proteins, and flavonoids, has been characterized through various analytical techniques, including high-performance liquid chromatography (HPLC) [37–40].

The aim of this study to develop an eco-friendly synthesis of cobalt oxide nanoparticles (CoO—NPs) using *Turmeric* ethanolic extract, comprehensively characterize their physicochemical properties, and evaluate their antioxidant, antibacterial, and anti-cancer potentials to advance sustainable nanotechnology and explore biomedical applications.

2. Methodology and procedures

2.1. Materials

$Co(NO_3)_2.6(H_2O)$, 291.03 g/mol (Sigma-Aldrich Chemie GmbH, USA). Turmeric powder (Assuit local market, Egypt), Ethanol HPLC gradient grade (ROTH, UK). All the rest of the chemicals and reagents were analytical grade (Loba Chemie, India).

2.2. Preparation of the turmeric extract

The methodology was adopted according to the previously prepared method by Basima et al. [41]. The alcoholic extract of 28 % w/v turmeric powder and 3.5 % w/v polyethylene glycol 6000 was created in ethanol 70 % under a reflux system for 30 min at 70 °C. Subsequently, the solution was cooled and adjusted to be slightly alkaline using ammonium hydroxide 10 % v/v and filtered using Whatman filter paper no. 1 and subsequently stored in a refrigerator for future use.

2.3. Preparation of the biosynthesized cobalt oxide nanoparticles

A solution in molar concentration of 0.01 M from cobalt(II) nitrate hexahydrate was prepared in water forming a clear, blue solution. The cobalt solution was slowly added to the turmeric alcoholic extract in the ratio (1:3) in temperature reaction condition at 70 °C at constant stirring at 1200 rpm for three hours. Subsequently, the reaction mixture was centrifuged at 4000 rpm 5 times using purified water for washing the precipitate in the last two runs. The resultant nanoparticles were dried in a hot air oven at 120 °C for three hours giving metallic black powder.

2.4. Characterization of CoO—NPs

The biosynthesized CoO—NPs were thoroughly characterized using various spectroscopic techniques. The structural analysis was performed using an XRD pattern obtained from a diffractometer of X-ray (60PA-JSDX-Model-JEOL) from two Theta 4–90 degrees by step 0.2 degree, providing insights into their crystalline nature. Scanning Electron Microscopy (SEM) analysis, conducted using an SEM JEOL model JSM IT 200 equipped with an EDX analyzer, revealed the morphology and surface characteristics of the CoO—NPs. The functional groups responsible for the reduction and stabilization of turmeric were identified using an ATR Thermo Fisher model Nicolet iS10 FT-IR spectrometer in a wavenumber range of 4000–450cm^{-1}, offering valuable information about the chemical interactions and adsorbed some of the bioactive constituents of the extract. Additionally, an Ultraviolet-Visible (PerkinElmer Lambda 40 UV/Vis Spectrophotometer) was employed to determine the maximum absorption wavelength of the nanoparticles in the range of (300–800 nm), providing critical data for their optical properties. Transmission electron microscopy [TEM; JEOL model JEM-100 CXII], and the pH-meter Mettler Toledo model SevenMulti. The dynamic particle size and Zeta potential for the biosynthesized NMs were conducted using [NICOMP, NANO ZLS, Z3000 ZLS].

2.4.1. UV–vis and bandgap energy equations

The band structure and the transition of electron type can be investigated using the following equation:

$$\alpha = 2.303 * A/d \quad (1)$$

Where; α is the absorption coefficient, d is the thickness of the sample, and A is the absorbance.

The energy band gap (E_g) of the as-biosynthesized CoO—NPs can be determined using the Tauc equation:

$$(\alpha h\upsilon)^n = C(h\upsilon - E_g) \quad (2)$$

Where; α is the absorption coefficient, hυ is the photon energy. n is assumed values of 2 and 0.5 for direct and indirect transitions, respectively, C is energy independent constant and E_g is the energy band gap of the CoO—NPs.

2.4.2. Scherrer equation [42,43]

$$D_{scher} = 0.9\lambda / \beta_{hkl}\cos(\theta_{hkl}) \quad (3)$$

Where 0.9 is a Scherrer constant;

λ is the radiation X-ray wavelength (CuKα= 1.541838 Å);

β_{hkl} is the full width at half maxima "FWHM" of the measured peaks, which were estimated and corrected according to the pseudo-Voigt function of the line profile relation.

θ_{hkl} is the degree of observed distinct diffraction peak in the XRD diffraction pattern.

2.5. Free radical scavenging activity using 2,2-diphenyl-1-picrylhydrazyl (DPPH) assay

The assay method was performed as AlSalhi et al. reported with slight modifications [44]. Multiple concentrations of each turmeric and CoO—NPs, ranging from 0.025 to 10 mg/mL in methanol, were prepared in methanol. For 0.2 mL of each concentration of turmeric and CoO—NPs, they mixed with a larger volume (1.8 mL) of the 0.1 mM DPPH. These mixtures allow the antioxidant components in the turmeric and CoO—NPs to interact with the DPPH radicals. The mixtures were shaken to ensure thorough mixing and left at room temperature for 30 min. During this time, any antioxidant compounds in both turmeric and CoO—NPs would neutralize the DPPH radicals. After incubation, solutions were measured at 517 nm using a spectrophotometer. BHT, a well-known synthetic antioxidant, was used as a positive control to provide a benchmark for comparison. By analyzing the results, the IC_{50} value was calculated (the concentration of both turmeric and CoO—NPs required to neutralize 50 % of the DPPH radicals).

$$\text{DPPH scavenging}(\%) = (A - B)/A \times 100 \quad (4)$$

Where A refers to negative control absorbance (DPPH solution in methanol) and B points to sample absorbance (the mixture of DPPH, methanol, and sample).

2.6. Antibacterial activity

This study aimed to investigate the antibacterial potential of newly biosynthesized CoO—NPs against bacterial standard strains. The study utilized vancomycin as a positive control and turmeric extract as a negative control. The tested strains included the Gram-positive bacterium (*B. subtilis*) and the Gram-negative bacterium (*E. coli*).

The antibacterial activity of CoO—NPs was evaluated using the agar well diffusion method. Six different concentrations (156.25, 312.5, 625, 1250, 2500, and 5000 ppm) were prepared of CoO—NPs and tested for their antibacterial efficacy.

To conduct the antibacterial activity bioassay, 1 mL of the prepared inocula of the standard strains was adjusted to a 0.5 McFarland turbidity standard. The inocula were then evenly spread onto Muller Hinton agar plates for bacteria [45]. Subsequently, 80 µL of each nanoparticle concentration was added to individual wells using a micropipette. The inoculated plates for bacterial strains were incubated at 37 °C for 24 h [46,47]. The antibacterial activity was assessed by measuring the diameter of the inhibition zone formed around the wells.

2.7. Anti-cancer activity

The MTT assay was employed to assess the cell proliferation of two human cancer cell lines: Caco-2 and MCF-7. These cell lines were obtained from the Science Way Company. The experimental procedures followed the protocols established in previous studies by Al-Hakkani et al. [43,48]. The cytotoxicity profile of the CoO—NPs was evaluated across a range of concentrations, from 3.125 to 100.0 µg/mL. A visible spectrophotometer, set at a wavelength of 560 nm, was utilized to measure the activity and assess the cytotoxic effects on the cancer cell lines.

3. Results and discussion

3.1. ATR-FTIR analysis

The emergence of green synthesis techniques in nanomaterial fabrication has garnered significant attention, particularly in the development of CoO—NPs using biological reducing agents. This study explores the intricate molecular interactions and structural transformations during the biosynthesis of CoO—NPs mediated by turmeric plant extract, utilizing ATR spectroscopy as a pivotal analytical technique.

The ATR-FTIR analysis (Fig. 1) of the turmeric plant extract revealed a complex molecular landscape, characterized by characteristic transmittance bands at critical wavenumbers 3263 cm^{-1}, 2916 cm^{-1}, 1594 cm^{-1}, 1387 cm^{-1},1259 cm^{-1}, 1020 cm^{-1} which could be attributed to O—H stretching vibrations, aliphatic C–H stretching, *C═O* carbonyl group vibration, O–H bending, unsaturated bond of *C═C*, and C—N stretching vibrations, respectively [8,34]. On the other hand, the biosynthesized CoO—NPs demonstrated a nuanced spectral evolution, with key bands at 3267 cm^{-1}, 2923 cm^{-1}, 1627 cm^{-1}, 1015 cm^{-1}, 656 cm^{-1}, 551 cm^{-1} which were caused by the presence of hydroxyl group interactions, modified aliphatic C—H stretching, shifted aromatic vibrations, *C═O* stretching, C—N band, metal-oxygen bond configurations of tetrahedral Co^{2+}—O^{2-} and characteristic of Co—O lattice vibrations of octahedral Co^{3+}—O^{2-}, respectively. These findings were found to agree with previously conducted papers on the biosynthesis of CoO—NPs using different plant extracts [4,49].

The comparative spectroscopic analysis unveils the intricate molecular transformations occurring during the green synthesis process, highlighting the critical role of turmeric plant extract in the controlled formation of CoO—NPs.

3.2. UV–Vis analysis

A comprehensive literature review of biosynthesized CoO—NPs published within the past five years reveals nuanced variations in maximum wavelengths. Recent scientific publications demonstrate absorption peaks ranging from 265–510 nm, positioning our 417 nm wavelength within the contemporary nanomaterial synthesis spectrum (Fig. 2**a**). Some research papers reported the maximum wavelengths of the biosynthesized CoO—NPs as Kumar et al. at maximum absorbance of 510 nm [50], Mudaliar et al. observed absorption peak at 265 nm [51]. Kavica et al. using *Ziziphus oenopolia* reported the absorption peak at 269 nm [52]. Our observed 417 nm wavelength demonstrates remarkable alignment with the most recent biosynthetic approaches, suggesting consistent optical characteristics across contemporary nanomaterial

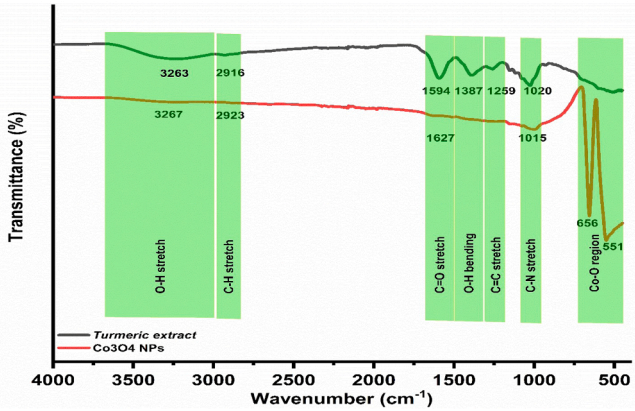

Fig. 1. ATR-FTIR spectra of turmeric and CoO—NPs.

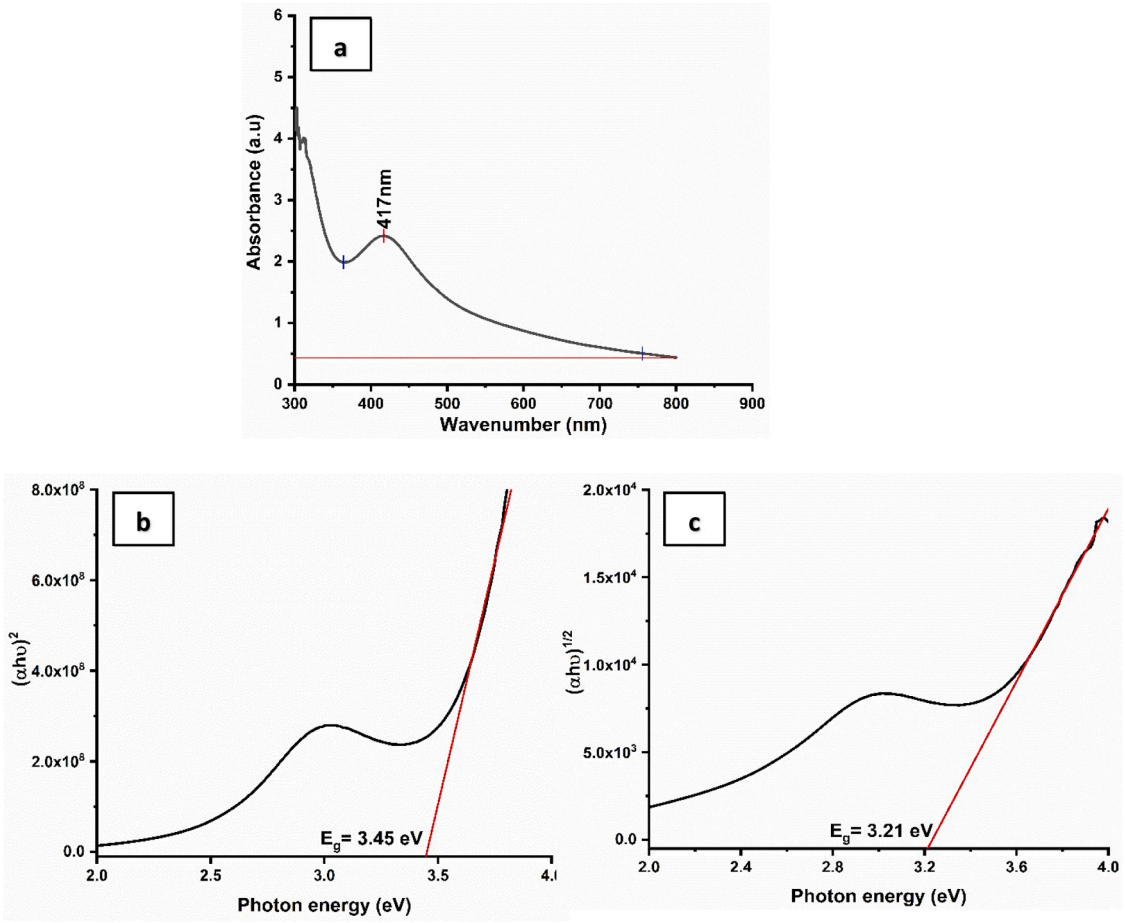

Fig. 2. a) UV–Vis spectrum of CoO—NPs, Tauc relationship of b) direct and c) Indirect band gap energy.

synthesis methodologies.

In general, the Co_3O_4 is an important semiconductor as a p-type with a direct energy band gap (E_g) of 3.95–2.13 eV [53] with bulk material E_g around 2.85 eV [54]. In the current study, using band structure and Tauc equations (Eq. (1) and Eq. (2)), the calculated E_g of 3.45 eV (primary transition pathway) represents a significant contribution to the understanding of electronic structural transitions in biosynthesized CoO—NPs (Fig. 2**b**). Comparative literature review reveals *piper betle* extract synthesis E_g at 3.86 eV [50], *Cordia myxa* extract method E_g at 2.42 eV [55], and spent-coffee-mediated extract approach revealed E_g at 3.09 eV [54].

The direct E_g value closely aligns with state-of-the-art biosynthetic methodologies, indicating the robust nature of the turmeric plant extract-mediated synthesis approach. The indirect E_g of 3.21 eV (secondary electronic transition mechanism) provides additional insights into the electronic structural characteristics, revealing subtle variations in electronic transition mechanisms (Fig. 2**c**). So, it is clear that in our approach we could manifest consistent optical properties across biosynthetic methodologies, potential for controlled electronic structural engineering, and demonstration of turmeric plant extract-mediated synthesis precision.

The comparative evaluation of direct and indirect E_g provides critical insights into the crystalline nature of the as-prepared CoO—NPs, substantiated by the research of Al-Hakkani et al. [43]. The observed phenomenon of direct E_g energy exceeding the indirect transition energy offers a fundamental understanding of the material's electronic structure.

Zimmermann et al. [56] documented Hematite's bulk E_g at 2.1 eV, providing a critical reference point for nanoscale electronic transition analysis. Also, he has proven that the change in the atomic electronic structure, increasing the E_g, indicates that the size of the particles has decreased, particularly towards the nanoscale. Al-Hakkani et al. confirmed this fact when they reported the E_g of hematite NPs using *Echinacea* in the range of 2.83–3.75 eV [43]. The comparative assessment revealed that direct electronic transitions predominate, demonstrating a direct correlation between absorption mechanisms and quantum confinement effects. So, key mechanistic insights could be gained by interpreting the quantum confinement effect as the fundamental mechanism driving electronic transition modifications, which emerges from nanoscale dimensional constraints and generates intragap electronic states. The estimated E_g values suggest the CoO—NPs exhibit remarkable semiconductor characteristics, characterized by enhanced optical responsiveness, sophisticated electrical property modulation, and potential for advanced electronic device applications.

3.3. XRD analysis

XRD examination provides critical insights into material properties, including crystallite dimensions, phase purity, crystallographic orientation, and structural integrity of the synthesized nanomaterials.

The synthesized CoO—NPs demonstrated a diffraction pattern with multiple characteristic peaks, revealing a crystalline structure. The XRD diffractogram (Fig. 3) exhibited eight distinct diffraction peaks at precise two-theta angles as 19.4°, 31.2°, 36.8°, 38.6°, 45.0°, 59.4°, and 65.4°, each representing specific crystallographic planes of the cobalt oxide structure which corresponded Miller indices "hkl" of 111, 220, 311, 222, 400, 511, 440, respectively. An additional carbon-related peak was observed at 28.6°, potentially indicating residual of some organic components from the biological synthesis process resulted after heating [57–59].

The two theta positioning and relative intensities of these diffraction

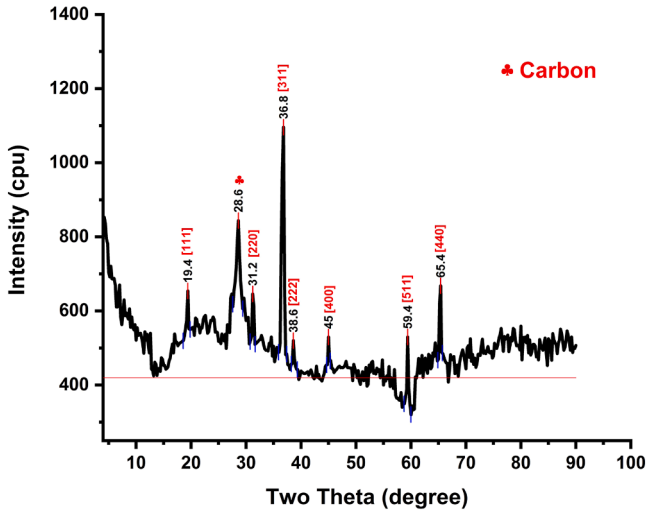

Fig. 3. XRD pattern of CoO—NPs.

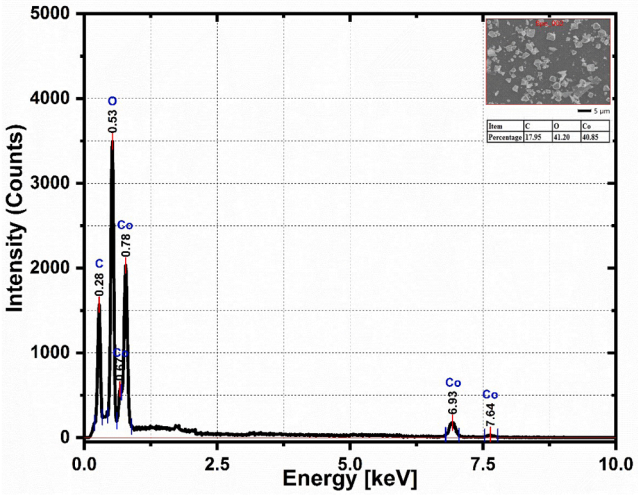

Fig. 4. EDX analysis of CoO—NPs.

peaks provide critical information about the CoO—NPs' crystallographic configuration. The systematic arrangement of peaks suggests a well-defined crystalline structure, indicative of the controlled nature of the biologically mediated synthesis approach.

Preliminary analysis indicates the presence of a predominantly cubic structure characteristic of CoO—NPs with unit cell $a = 8.0650$ Å which was agreed with the reference card# 00–153–8531, with potential minor structural noises introduced by the biological synthesis methodology. Also, the diffractogram was found to be compatible with previously reported by Savitha et al. [60].

The most abundant peak is the principal peak in the as-biosynthesized CoO—NPs with a crystallite size of 15.2 nm at Miller indices (311), where the average crystallite sizes for all of the peaks were found to be 31.2 nm as it was calculated using the Scherrer equation (Eq. (3)). Peak sharpness and resolution suggest high crystallinity, while peak breadth confirms the nanoscale material dimensions.

3.4. EDX analysis

Energy-dispersive X-ray (EDX) spectroscopy provides a critical window into the elemental composition and structural characteristics of CoO—NPs synthesized through innovative turmeric plant extract-mediated biosynthesis. This analytical technique offers precise quantification of material constituents, revealing the intricate chemical landscape of the synthesized nanomaterials. Analytical parametric conditions were adjusted at accelerating Voltage: 10.0 kV, magnification: 2700x, and imaging Scale: 5 $^{\mu m}$ (Fig. 4). The EDX examination unveiled a distinctive elemental composition as carbon;17.95 %, oxygen; 41.20 %, and cobalt; 40.85 %. The elemental distribution provides critical insights into the biosynthesis process, highlighting the intricate interplay between organic and inorganic components. The significant presence of carbon (17.95 %) suggests residual organic moieties from the turmeric plant extract, potentially serving as stabilizing agents during nanoparticle formation [58,59]. The oxygen content (41.20 %) corroborates the expected stoichiometry of cobalt oxide, while the cobalt representation (40.85 %) confirms the primary structural composition of the nanomaterial.

The sharpness of the peaks revealed the high crystallinity nature which confirm the XRD results. The precise elemental mapping demonstrates the sophisticated control achieved through green synthesis methodologies. The near-stoichiometric balance between oxygen and cobalt underscores the remarkable precision of the biologically mediated synthesis approach, bridging the gap between natural processing and advanced nanomaterial engineering. The EDX analysis provides unequivocal evidence of the successful biosynthesis of CoO—NPs, showcasing the potential of plant extract-mediated synthesis in generating precisely engineered nanomaterials with controlled elemental composition.

3.5. Dynamic light scattering (DLS) and Zeta potential measurements

The biosynthesized CoO—NPs exhibited a hydrodynamic diameter of 86.29 nm, representing the ensemble-averaged particle size in liquid suspension (Fig. 5**a**). This dimensional measurement encompasses not only the core nanoparticle structure but also the hydration layer and associated stabilizing biomolecules derived from the turmeric plant extract. The Polydispersity Index (PDI) of 0.38 indicates a moderate heterogeneity in particle size distribution. While this value exceeds the ideal threshold of 0.2 but not more than 0.4, it suggests potential variability in nanoparticle synthesis conditions. The PDI provides critical insight into the uniformity of the synthesized nanomaterial, with higher values indicating increased size heterogeneity and potential challenges in achieving uniform nucleation and growth mechanisms.

Zeta potential measurement revealed a negative surface charge of −21.66 mV, which provides crucial information about the colloidal stability and surface chemistry of the biosynthesized CoO—NPs (Fig. 5b). The observed negative charge suggests significant surface functionalization, likely attributed to the organic capping agents present in the turmeric plant extract. The zeta potential magnitude approaches, but marginally falls short of, the optimal ±25 mV threshold typically associated with maximal colloidal stability. The negative charge indicates electrostatic repulsion mechanisms that mitigate particle aggregation, though the relatively moderate value suggests potential limitations in long-term colloidal suspension maintenance.

The data on hydrodynamic diameter, polydispersity index, and zeta potential together reveal the intricate surface chemistry and stabilization processes involved in this nature-inspired nanoparticle synthesis method. The turmeric plant extract seems key in influencing the nanoparticles' surface characteristics, offering control over their size and some degree of electrostatic stability.

3.6. TEM and SEM analyses

Transmission Electron Microscopy (TEM) dimensional characterization (Fig. 6**a**) was conducted to unveil the particle size distribution (Fig. 6**b**) of the CoO—NPs giving a mean particle size of 26.3 nm, standard deviation of 5.6 nm, minimum particle size of 14.0 nm, median of 26.6 nm, and maximum particle size of 38.4 nm. The TEM analysis revealed a narrow size distribution characteristic of the controlled

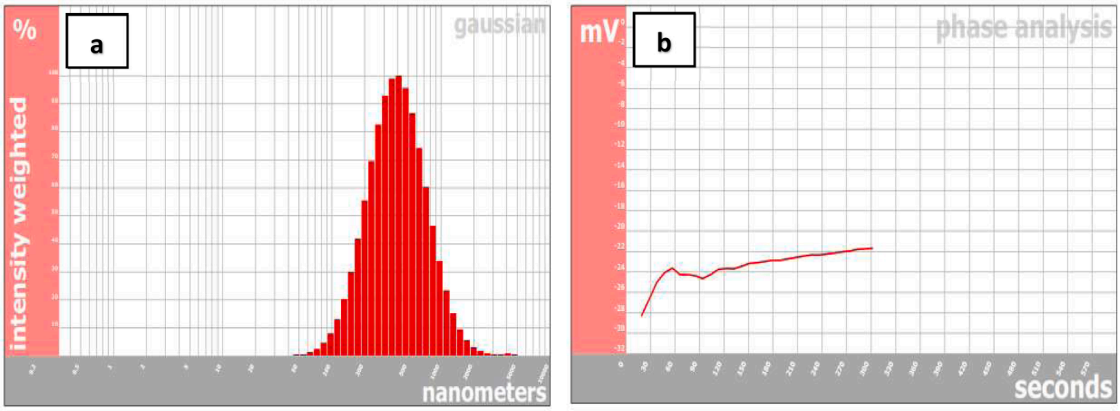

Fig. 5. a) DLS analysis and b) Zeta potential of CoO—NPs.

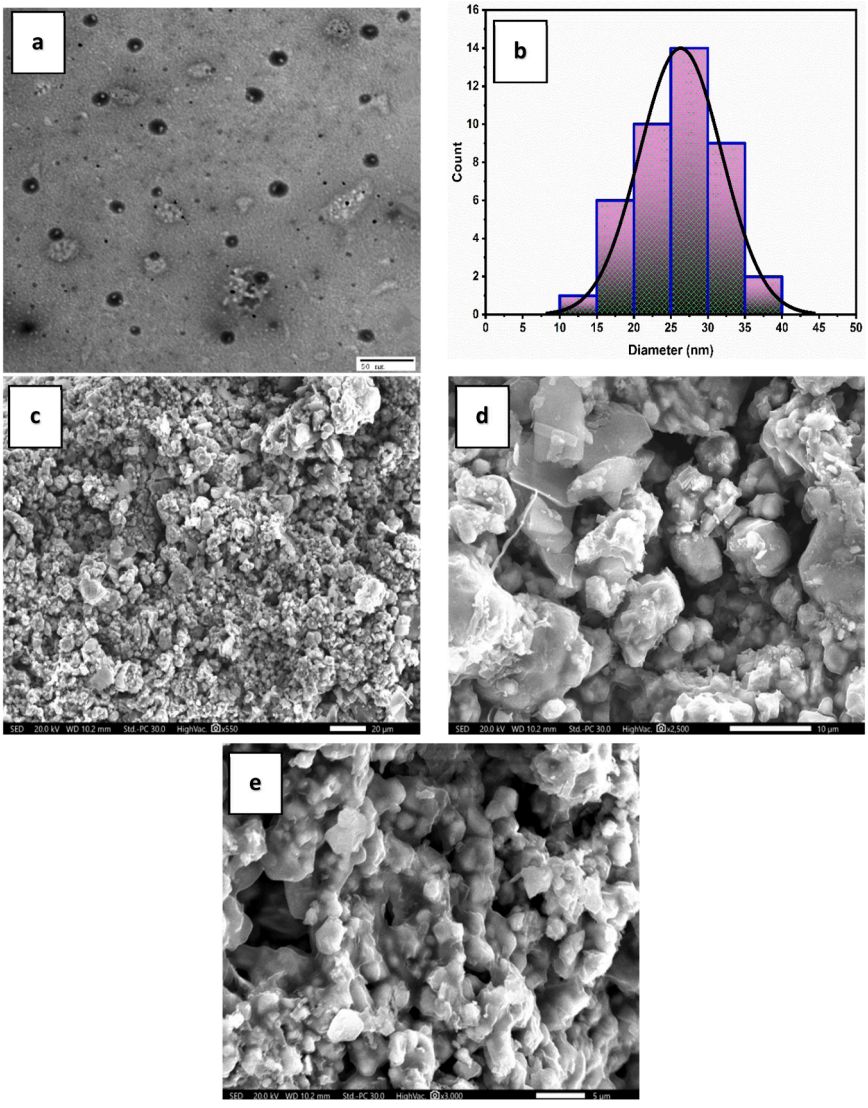

Fig. 6. a) TEM analysis at scale image 50 nm, b) particle size distribution, SEM analysis at image scales c) 20 μm, d) 10 μm, and 5 μm of CoO—NPs.

biosynthesis process. The relatively low standard deviation (5.6 nm) indicates remarkable uniformity in CO—NP nucleation and growth mechanisms mediated by the turmeric plant extract. The size range spanning from 14.0 nm to 38.4 nm suggests a consistent yet slightly heterogeneous population of CoO—NPs.

Scanning Electron Microscopy (SEM) morphological was also conducted at three different parameters of image scale as follows, first imaging configuration (magnification of 550X and scale of 20 μm)

(Fig. 6**c**). Second imaging configuration (magnification of 2500X and scale of 10 μm) (Fig. 6**d**), the third one at (magnification of 3000X and scale of 5 μm) (Fig. 6**e**) at the same accelerating voltage of 20 kV for each. The SEM analysis of the CoO—NPs unveiled a complex surface topography characterized by rough surface morphology, intricate surface textures as cubic structural elements, and heterogeneous surface features with intermittent spatial variations. Also, the microscopic examination revealed a multifaceted surface structure with spherical and semi-spherical particles and irregular surface contours present in intergranular spaces with potential agglomeration tendencies and microscale architectural complexity.

The combined TEM and SEM analysis provides comprehensive insights into the morphological and dimensional properties of biosynthesized CoO—NPs. The controlled synthesis approach mediated by turmeric plant extract demonstrates remarkable capability in generating nanoparticles with consistent size distribution and controlled morphological characteristics, with the potential for advanced functional applications with tailored physicochemical properties. These properties make the CoO—NPs a good platform for catalytic and adsorption techniques for the removal of either organic or inorganic contaminations from wastewater.

3.7. Determination of the antioxidant activity

DPPH serves as a standard model for free radicals. The DPPH solution has a distinctive purple color and is typically used to assess the antioxidant capacity of various compounds. After antioxidant neutralization with the DPPH radicals, the purple color of the solution fades to convert into a yellow color at increasing concentration. This new color change formation may be attributed to accepting hydrogen or an electron. The intensity of the changed color was quantified by measuring the change in light absorption. The DPPH assay is a highly valuable and significant method for detecting antioxidant properties in turmeric and CoO—NPs. This assay is not only simple and cost-effective but also provides successive results. IC_{50} values were calculated, and they were found to be 3.82 mg/mL and 1.171 mg/mL for turmeric and CoO—NPs against DPPH radical scavenging activity, respectively, while BHT showed 0.42 mg/mL IC_{50} value. The reasonable IC_{50} value of CoO—NPs enables them to carry out other activities directly related to entering living cells, such as bacteria, fungi, and cancer cells, and causing mutations within them. This suggests the potential use of these nanoparticles as antibacterial or anti-cancer agents where the substances have antioxidant activity and play a crucial role in protecting cells from oxidative stress, which is linked to various chronic diseases and aging processes.

3.8. Antibacterial activity

Biosynthesized CoO—NPs were evaluated for their antibacterial properties against two distinct bacterial types: Gram-negative *(E. coli)* and Gram-positive *(B. subtilis)*. *E. coli*, a Gram-negative bacterium, possesses a complex cell wall structure comprising three layers: mucopeptide (peptidoglycan), a lipoprotein layer, and a lipopolysaccharide layer. This intricate composition includes a higher concentration of amino acids and lipids [45]. In contrast, Gram-positive bacteria, such as *B. subtilis*, exhibit a simpler cell wall structure consisting of only two layers: mucopeptide (peptidoglycan) and teichoic acid [47]. The absence of an outer membrane and the presence of a thicker peptidoglycan layer render Gram-positive bacteria more susceptible to certain nanoparticles.

The study aimed to explore the relationship between nanoparticle characteristics and their antibacterial efficacy. The antibacterial activity was assessed using inhibition zone diameters at various concentrations. Turmeric extract served as a negative control, demonstrating no activity, while vancomycin acted as a positive control, producing an inhibition zone of 19.3 mm at 10 ppm.

The CoO—NPs exhibited concentration-dependent inhibition against both bacterial types (Table 1). At the highest concentration of 5000 ppm, the CoO—NPs displayed impressive inhibition zones of 20.7 mm and 18.8 mm against *B. subtilis* and *E. coli*, respectively (Fig. 7). However, at the lowest concentration of 156.25 ppm, the inhibition zones decreased to 10.3 mm and 10.9 mm for *E. coli* and *B. subtilis*, respectively.

As shown in (Table 1), the impact of biogenically synthesized CoO—NPs on *B. subtilis* is more pronounced compared to its effect on *E. coli*. This difference in efficacy could be attributed to the distinct structural composition of these bacterial types, as previously mentioned. It is easier for CoO—NPs to penetrate the cell wall of Gram-positive bacteria, leading to greater destruction of cellular proteins and nucleic acids. In contrast, the impact on Gram-negative bacteria is relatively less significant.

This variation in the antibacterial activity of CoO—NPs is likely due to the different structural characteristics of Gram-positive and Gram-negative bacteria. The ability of CoO—NPs to effectively penetrate the cell wall and interact with the cellular components is influenced by the bacterial type. The enhanced destruction of proteins and nucleic acids in Gram-positive bacteria further contributes to the observed differences in antibacterial efficacy.

The superior performance of CoO—NPs in penetrating the complex cell walls of both Gram-negative and Gram-positive bacteria may be attributed to their reduced particle size at the nanoscale. This size reduction facilitates more efficient penetration, enhancing the nanoparticles' antibacterial potential.

So, specific further research is warranted to explore the specific mechanisms underlying the differential impact of CoO—NPs on Gram-positive and Gram-negative bacteria. Understanding these mechanisms could provide valuable insights for developing targeted antibacterial strategies and optimizing the use of CoO—NPs in various applications.

The minimum inhibition concentration (MIC) could be calculated theoretically using the microbial assay equation as follows:

$$\textbf{Inhibition zone (mm)} = \textbf{(s)} \times \textbf{ln (concentration)} + \textbf{(u)}$$

Where, s is the slope of the linear relationship, u is the intercept.

$$\textbf{MIC} = e^{((6.1 - (u))/s)}$$

Where 6.0 mm is the well diameter in mm and 6.1 mm is the smallest diameter could give an inhibition effect.

As Fig. 8 manifested, there were a directly proportional relationship between inhibition zone and ln (concentration) where in CoO—NPs the regression line coefficients revealed high linearity with $R^2 > 0.90$ according to the validation methodology guidelines for linear equations especially, for microbial assay. So, according to the depicted equations in the (Fig. 8), the MIC was 25.3 ppm and 22.8 ppm for *B. subtilis* and *E. coli*, respectively.

3.9. Anti-cancer activity

The MTT assay revealed distinctive cytotoxic responses of CoO—NPs across two human adenocarcinoma cell lines of MCF-7 and Caco-2. The comprehensive concentration-dependent analysis demonstrated

Table 1
The antibacterial activity of the as-prepared CoO—NPs against *B. subtilis* ATCC 6633 and *E. coli* ATCC 8739 bacterial standard strains.

Concentration (ppm)	*E. coli* Inhibition zone (mm)	*B. subtilis*
5000	18.8 ± 0.2	20.7 ± 0.3
2500	17.0 ± 0.5	19.0 ± 0.2
1250	16.9 ± 0.3	17.4 ± 0.4
625	13.6 ± 0.8	14.3 ± 0.4
312.5	12.8 ± 0.8	13.8 ± 0.6
156.25	10.3 ± 0.5	10.9 ± 0.8

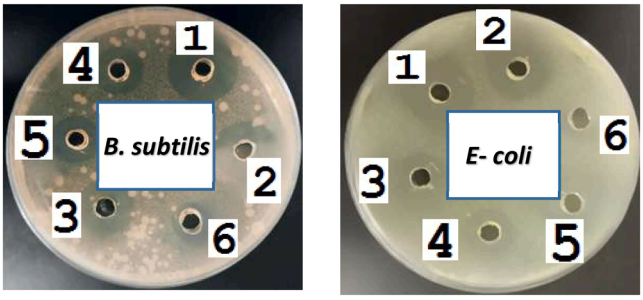

Fig. 7. Antibacterial activity of the as-biosynthesized CoO—NPs against *B. subtilis* ATCC 6633 and *E. coli* ATCC 8739 at different concentrations of 1) 5000 ppm, 2) 2500 ppm, 3) 1250 ppm, 4) 625 ppm, 5) 312.5 ppm, and 6) 156.25 ppm.

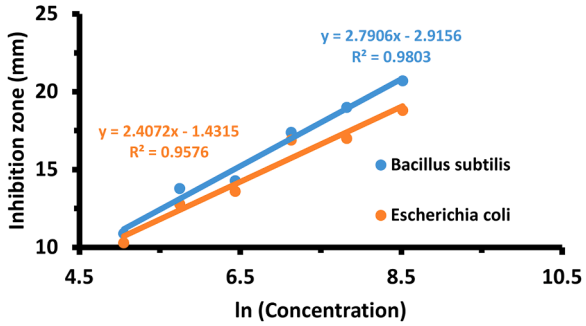

Fig. 8. Microbial assay relationship of the as-biofabricated CoO—NPs against *B. subtilis* and *E. coli* bacterial standard strains at different concentrations in the range of 5000 ppm-156.25 ppm.

significant cellular metabolic inhibition mechanisms. The precise IC_{50} determination unveiled cell line-specific sensitivity where it was found to be 26.4 μg/mL and 43.6 μg/mL for Caco-2 and MCF-7 cell lines, respectively (Fig. 9).

The markedly lower IC_{50} for Caco-2 cells indicates heightened susceptibility to CoO—NPs when compared with some of the other papers, suggesting potential line-specific molecular vulnerability mechanisms (Table 2). One of the potential mechanisms can be ROS generation. Nanoparticle-induced cellular damage predominantly manifests through robust ROS generation.

The nanoscale morphology of CoO—NPs critically influences oxidative stress induction. This action can be attributed to surface reactivity dynamics, where increased surface area-to-volume ratio, enhanced electron transfers capabilities, and accelerated free radical production.

Table 2
Comparison of the anti-cancer activity of the as-prepared CoO—NPs against some previously published papers.

Plant	Cell line type	IC_{50} (μg/mL)	Ref.
Psidium guajava Leaves	HCT 116	24.5	[61]
	MCF-7	29.5	
Turmeric	Caco2	26.4	Current study
	MCF-7	43.6	
Chemical reduction method	MCF-7	30.8	[1]
Prickly pear fruit	HepG2	100	[15]
Caccinia Macranthera seeds	Huh-7	375	[25]

Also, oxidative stress cascades through mitochondrial electron transport chain disruption, glutathione system overwhelming, lipid peroxidation initiation, and protein oxidative modification.

Nanoscale structural implications are considered the main motive for anti-cancer activity in our opinion where the sub-100 nm particle dimensions the responsible for facilitating unprecedented cellular interaction mechanisms. This nature enhanced membrane penetration, improved intracellular distribution, and amplified biochemical reactivity.

The differential IC_{50} values suggest intrinsic molecular variations where Caco-2 is more vulnerable to cellular architecture while, MCF-7 has relatively enhanced stress tolerance mechanisms.

4. Conclusion

This study establishes the efficacy of a green biosynthesis method for cobalt oxide nanoparticles (CoO—NPs) using turmeric ethanolic extract, offering a scalable, environmentally benign alternative to conventional chemical synthesis that minimizes ecological impact while advancing nanomaterial innovation. The multifaceted characterization reveals that the extract not only facilitates precise control over nanoparticle size, morphology, and surface chemistry but also enhances stability through functional group capping and electrostatic interactions, underscoring the potential of plant-derived agents in tailoring nanomaterial properties for targeted applications. Notably, the synthesized CoO—NPs demonstrate enhanced antioxidant capabilities surpassing those of the raw extract, alongside robust antibacterial action against both Gram-positive and Gram-negative pathogens, and promising anticancer effects via ROS-mediated mechanisms, positioning them as versatile candidates for biomedical interventions. Overall, this work propels sustainable nanotechnology forward by validating bio-inspired routes for high-performance nanomaterials, illuminating their therapeutic promise in fields like medicine and materials engineering, and advocating for rigorous toxicity evaluations to bridge the gap toward safe clinical and antimicrobial deployment, thereby opening avenues for

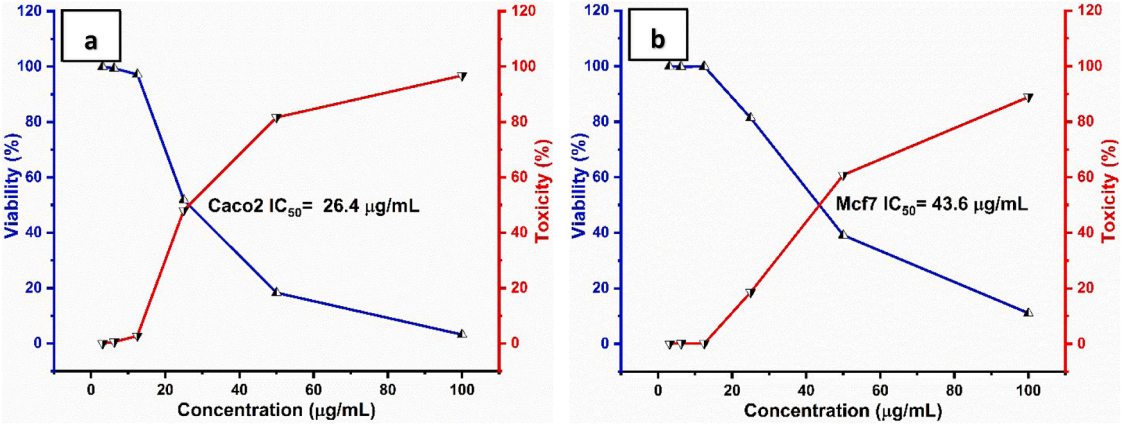

Fig. 9. Anti-cancer activity of the as-biosynthesized CoO—NPs against a) Caco-2 and b) MCF-7 cell lines in the range concentration of 3.125–100μg/mL.

interdisciplinary research in eco-conscious material design.

Experimental work and methods

We confirm that all methods were carried out following relevant guidelines and regulations.

Ethics approval and consent to participate

Paper is not involving human participants or animals.

Consent for publication

Not applicable.

Availability of data and materials

All data generated or analyzed during this study are included in this paper.

Funding

This research paper did not have any external funding.

Generative AI and AI-assisted technologies in the writing process

During the preparation of this work, the authors used Grammarly, Inc. and Cohere websites for English language enhancement.

CRediT authorship contribution statement

Mais Mazin Al-Hamdani: Visualization, Methodology, Investigation, Data curation, Conceptualization. **Basima A.A. Saleem:** Writing – original draft, Visualization, Methodology, Investigation, Data curation. **Mohammed Ihsan Majeed:** Visualization, Investigation, Data curation. **Mohamed Ahmed:** Writing – review & editing, Supervision. **Helal F. Hetta:** Visualization, Resources, Investigation, Funding acquisition. **Mohammed S. Saddik:** Visualization, Investigation. **Stefan Bräse:** Writing – review & editing, Supervision, Funding acquisition, Conceptualization. **Mostafa F. Al-Hakkani:** Writing – original draft, Validation, Methodology, Conceptualization.

Declaration of competing interest

The authors declare that they have no known competing financial interests or personal relationships that could have appeared to influence the work reported in this paper.

Acknowledgments

The corresponding authors gratefully acknowledge to the members of the Stefan Bräse group for their valuable support.

Data availability

Data will be made available on request.

References

[1] P. Meyyathal, N. Santhiya, S. Umadevi, Preparation of Co3O4 nanoparticles in a lyotropic liquid crystal medium and their application in anti-bacterial, anti-cancer and catalytic activities, J. Bionanosci. 14 (2024) 1293–1303.
[2] D.T. Tefera, T.D. Zeleke, Green synthesis, characterization, and evaluation of antimicrobial and antioxidant activities of CuO, Co 3 O 4, and CuO-Co 3 O 4 nano system using Moringa stenopetala plant leaf extracts, Nanomed. J. 11 (3) (2024) 294–310.
[3] P.R. Bhilkar, R.S. Madankar, A.R. Chaudhary, R.R. Chaudhary, S.R. Somkuwar, A. K. Potbhare, K. Dadure, A.A. Abdala, R.G. Chaudhary, Biosynthesis of microrubble-shaped nanoporous Co3O4/rGO NCs using leaves extract of Neolamarckia cadamba and its antibacterial/antioxidant performance, Nano-Struct. Nano-Objects 39 (2024) 101291.
[4] P.D. Sarvalkar, A.S. Jamadar, A.B. Magdum, P.K. Pawar, J.B. Yadav, M. S. Nimbalkar, N.R. Prasad, A.A. Ramteke, K.K.K. Sharma, Biogenic synthesis of Co3O4 nanoparticles from Aloe barbadensis extract: antioxidant and antimicrobial activities, and photocatalytic degradation of azo dyes, Results. Eng. 22 (2024) 102094.
[5] M.S. AlSalhi, G. Oza, I. Castillo-Maldonado, A. Sharma, Evaluation of antimicrobial, antioxidant, and anti-inflammatory abilities of sustainably synthesized Co3O4 NPs, Biocatal. Agric. Biotechnol. 56 (2024) 103025.
[6] M.K. Shumete, L.T. Tufa, F.K. Sabir, H.A. Murthy, E.T. Bekele, B.A. Gonfa, Synthesis of Co3O4 nanoparticles using Ananas Comosus Peel extract for Cr6+ ion adsorption and antibacterial applications, Chem. Select. 9 (45) (2024) e202403797.
[7] Y. Huang, W. Liao, W. Wang, T. Zhang, Y. Zhang, L. Lu, Facile synthesis of nanoparticles-stacked Co3O4 nanoflakes with catalase-like activity for accelerating wound healing, Regen. Biomater. 11 (2024) rbae006.
[8] Z. Sabouri, S. Sammak, S. Sabouri, S. Moghaddas, M. Darroudi, Green synthesis of Ag-Se doped ZnO-Co3O4-NiO fivenary nanocomposite using poly anionic cellulose and evaluation of their anticancer and photocatalyst applications, Chem. Methodol. 8 (3) (2024) 164–176.
[9] A.T. al Alawi, M.T. al Alawi, N.H. Roodbari, A. Es-haghi, M. Mashreghi, Biosynthesis of cobalt oxide nanoparticles and their cytotoxicity against cancer cells mouse colon adenocarcinoma cell line, Results. Chem. 11 (2024) 101839.
[10] S.R. Yousefi, H.A. Alshamsi, O. Amiri, M. Salavati-Niasari, Synthesis, characterization and application of Co/Co3O4 nanocomposites as an effective photocatalyst for discoloration of organic dye contaminants in wastewater and antibacterial properties, J. Mol. Liq. 337 (2021) 116405.
[11] N.K. Yetim, E.H. Özkan, H. Öğütçü, Use of Co3O4 nanoparticles with different surface morphologies for removal of toxic substances and investigation of antimicrobial activities via in vivo studies, Environ. Sci. Pollution Res. 30 (48) (2023) 106585–106597.
[12] D. Dayal Upadhyay, S. Singh, K. Bahadur Singh, N. Gautam, S. Shrivastava, G. Pandey, Biogenically produced Co3O4 nanoparticles and their application as micronutrient and antimicrobial agent for agro-environmental sustainability, Inorg. Chem. Commun. 155 (2023) 110957.
[13] R. Kumar, K. Kumar, N. Thakur, M.S. Chauhan, Harnessing microwaves for the biosynthesis of CuO-Co3O4 NCs: a dual study on photocatalytic process and antibacterial effectiveness, Int. J. Environ. Anal. Chem. (2023) 1–20.
[14] C.T. Anuradha, P. Raji, Facile-synthesis and characterization of cobalt oxide (Co3O4) nanoparticles by using Arishta leaves assisted biological molecules and its antibacterial and antifungal activities, J. Mol. Struct. 1262 (2022) 133065.
[15] M.D. Nagajothi, J. Maheswari, Biosynthesis and characterization of Co3O4NPs utilizing prickly pear fruit extract and its biological activities, J. Turkish Chem. Society Sect. A: Chem. 9 (4) (2022) 1117–1128.
[16] T. Athar, A. Hakeem, N. Topnani, A. Hashmi, Wet synthesis of monodisperse cobalt oxide nanoparticles, Int. Sch. Res. Notices. 2012 (1) (2012) 691032.
[17] A.D. Khalaji, M. Nikookar, K. Fejfarova, M. Dusek, Synthesis of new cobalt(III) Schiff base complex: a new precursor for preparation Co3O4 nanoparticles via solid-state thermal decomposition, J. Mol. Struct. 1071 (2014) 6–10.
[18] J. Deng, L. Kang, G. Bai, Y. Li, P. Li, X. Liu, Y. Yang, F. Gao, W. Liang, Solution combustion synthesis of cobalt oxides (Co3O4 and Co3O4/CoO) nanoparticles as supercapacitor electrode materials, Electrochim. Acta 132 (2014) 127–135.
[19] R. Pitcheri, S.P. Mooni, D. Radhalayam, M. Nora, S. Roy, F.A.M. Al-Zahrani, M. Suneetha, Effect of Ce-doping on the structural, morphological, and electrochemical features of Co3O4 nanoparticles synthesized by solution combustion method for battery-type supercapacitors, Ceram. Int. 50 (23, Part B) (2024) 50504–50515.
[20] N.M. Shaalan, M. Rashad, A.H. Moharram, M.A. Abdel-Rahim, Promising methane gas sensor synthesized by microwave-assisted Co3O4 nanoparticles, Mater. Sci. Semicond. Process. 46 (2016) 1–5.
[21] C.R. Babu, A.V. Avani, S. Shaji, E.I. Anila, Electrochemical characteristics of Co3O4 nanoparticles synthesized via the hydrothermal approach for supercapacitor applications, J. Solid State Electrochem. 28 (7) (2024) 2203–2210.
[22] J. Pal, P. Chauhan, Study of physical properties of cobalt oxide (Co3O4) nanocrystals, Mater. Charact. 61 (5) (2010) 575–579.
[23] D. Barreca, C. Massignan, S. Daolio, M. Fabrizio, C. Piccirillo, L. Armelao, E. Tondello, Composition and microstructure of cobalt oxide thin films obtained from a novel cobalt(II) precursor by chemical vapor deposition, Chem. Mater. 13 (2) (2001) 588–593.
[24] E. Jang, H.-W. Shim, B.H. Ryu, D.R. An, W.K. Yoo, K.K. Kim, D.-W. Kim, T.D. Kim, Preparation of cobalt nanoparticles from polymorphic bacterial templates: a novel platform for biocatalysis, Int. J. Biol. Macromol. 81 (2015) 747–753.
[25] A. Mohandes, M. Reza Aghamaali, Z. Sabouri, M. Darroudi, Biosynthesis of cobalt oxide nanoparticles (Co3O4-NPs) using Caccinia Macranthera extract and evaluation of their cytotoxicity and photocatalytic activity, Mater. Sci. Eng.: B 297 (2023) 116782.
[26] F. Aslam, L.A. Minhas, M. Kaleem, A. Jabeen, A. Akram, H.A. Malik, H.M. U. Farooqi, M.W. Amin, A.S. Mumtaz, Sustainable synthesis of cobalt oxide nanoparticles (Co3O4-NPs) using extract of nodosilinea nodulosa: characterization and potential biological applications, J. Bionanosci. 14 (5) (2024) 4764–4778.
[27] M. Eltarahony, S. Zaki, M. ElKady, D. Abd-El-Haleem, Biosynthesis, characterization of some combined nanoparticles, and its biocide potency against a broad spectrum of pathogens, J. Nanomater. 2018 (1) (2018) 5263814.

[28] B.A. Omran, H.N. Nassar, S.A. Younis, R.A. El-Salamony, N.A. Fatthallah, A. Hamdy, E.H. El-Shatoury, N.S. El-Gendy, Novel mycosynthesis of cobalt oxide nanoparticles using Aspergillus brasiliensis ATCC 16404—Optimization, characterization and antimicrobial activity, J. Appl. Microbiol. 128 (2) (2020) 438–457.
[29] L. Han, D.-P. Yang, A. Liu, Leaf-templated synthesis of 3D hierarchical porous cobalt oxide nanostructure as direct electrochemical biosensing interface with enhanced electrocatalysis, Biosens. Bioelectr. 63 (2015) 145–152.
[30] T. Rasheed, F. Nabeel, M. Bilal, H.M.N. Iqbal, Biogenic synthesis and characterization of cobalt oxide nanoparticles for catalytic reduction of direct yellow-142 and methyl orange dyes, Biocatal. Agric. Biotechnol. 19 (2019) 101154.
[31] N. Matinise, N. Mayedwa, X.G. Fuku, N. Mongwaketsi, M. Maaza, Green synthesis of cobalt (II, III) oxide nanoparticles using Moringa Oleifera natural extract as high electrochemical electrode for supercapacitors, AIP. Conf. Proc. 1962 (1) (2018) 040005.
[32] A. Waris, M. Din, A. Ali, S. Afridi, A. Baset, A.U. Khan, M. Ali, Green fabrication of Co and Co3O4 nanoparticles and their biomedical applications: a review, 16(1) (2021) 14–30.
[33] D. Kharade Suvarta, H. Nikam Gurunath, J. Mane Gavade Shubhangi, R. Patil Sachinkumar, V. Gaikwad Kishor, Biogenic synthesis of cobalt nanoparticles using Hibiscus cannabinus leaf extract and their antibacterial activity, J. Res. J. Chem. Environ. 24 (5) (2020) 9–13.
[34] H.A. Pawar, B.S. Dhingra, Phytochemistry, applications and patents of Curcuma Longa (Turmeric): a comprehensive review, J. Advanc. Pharmacog. 4 (1) (2024).
[35] L. Frattaruolo, G. Lauria, F. Aiello, G. Carullo, R. Curcio, M. Fiorillo, G. Campiani, V. Dolce, A.R. Cappello, Exploiting glycyrrhiza glabra L. (Licorice) Flavanones: licoflavanone's impact on breast cancer cell bioenergetics, Int. J. Mol. Sci. (2024).
[36] A. Shakeri, Y. Panahi, T.P. Johnston, A. Sahebkar, Biological properties of metal complexes of curcumin, Biofactors 45 (3) (2019) 304–317.
[37] P.V. Kadam, K.N. Yadav, C.L. Bhingare, M.J. Patil, Standardization and quantification of curcumin from Curcuma longa extract using UV visible spectroscopy and HPLC, J. Pharmacog. Phytochem. 7 (5) (2018) 1913–1918.
[38] H.K. Syed, K.B. Liew, G.O.K. Loh, K.K. Peh, Stability indicating HPLC–UV method for detection of curcumin in Curcuma longa extract and emulsion formulation, Food Chem. 170 (2015) 321–326.
[39] P. Mallya, D.L. Yarlagadda, S. Lewis, A novel stability-indicating RP-HPLC method for the simultaneous estimation and In vitro and In vivo evaluation: curcumin and naringin Co-amorphous system, Food Anal. Methods 17 (5) (2024) 751–765.
[40] D. Eneş, M. Çelebier, D. Dikmen, S. Altınöz, RP-HPLC method development for determination of curcumin in commercial turmeric capsules, Hacettepe Univ. J. Faculty Pharmacy 44 (1) (2024) 1–8.
[41] B.A.A. Saleem, M.I. Majeed, M.S. Saddik, S.A. Elshanawany, S.H.A. Hassan, M. A. El-Mokhtar, H.F. Hetta, M.F. Al-Hakkani, Hydrothermal synthesis of MoO3, CeO2, and their nanocomposite for thymol blue adsorption, anticancer, and antibacterial activity, J. Bionanosci. 15 (3) (2025) 502.
[42] G. Madhu, V.C. Bose, K. Maniammal, A.A. Raj, V. Biju, Microstrain in nanostructured nickel oxide studied using isotropic and anisotropic models, Phys. B (Amsterdam, Neth.) 421 (2013) 87–91.
[43] M.F. Al-Hakkani, G.A. Gouda, S.H.A. Hassan, A.M. Nagiub, *Echinacea purpurea* mediated hematite nanoparticles (α-HNPs) biofabrication, characterization, physicochemical properties, and its in-vitro biocompatibility evaluation, Surf. Interfaces. 24 (2021) 101113.
[44] M.S. AlSalhi, G. Oza, I. Castillo-Maldonado, A. Sharma, Evaluation of antimicrobial, antioxidant, and anti-inflammatory abilities of sustainably synthesized Co3O4 NPs, Biocatal. Agric. Biotechnol. 56 (2024) 103025.
[45] M. Hassan, M. Ismail, A. Moharram, A. Shoreit, Synergistic effect of biogenic silver-nanoparticles with β lactam cefotaxime against resistant *Staphylococcus arlettae* AUMC b-163 isolated from T3A Pharmaceutical Cleanroom, Assiut, Egypt, Am. J. Microbiol. Res. 4 (2016) 132–137.
[46] M. Hassan, A. Moharram, M. Ismail, A. Shoreit, Biogenic silver nanoparticles of resistant Aspergillus flavus AUMC 9834 against some pathogenic microorganisms and its synergistic effect with the antifungal fluconazole, J. Basic Appl. Mycol. 6 (2015) 1–7.
[47] A. Moharram, M. Ismail, A. Shoreit, M. Hassan, Biodiversity of microbiota in cephalosporin-manufacturing environments at T3A factory, Assiut, Egypt, J. Basic Appl. Mycol. 5 (2014) 1–13.
[48] B.R. Alsehli, M.H.A. Hassan, D.S. Mohamed, M.S. Saddik, M.F. Al-Hakkani, Enhanced cytotoxic efficacy against MCF-7 and HCT116 cell lines and high-performance cefoperazone removal using biogenically synthesized CeO_2 nanoparticles, J. Mol. Struct. 1318 (2024) 139261.
[49] O.S. Karvekar, A.S. Vadanagekar, P.D. Sarvalkar, S.S. Suryawanshi, S.M. Jadhav, R. D. Singhan, J.P. Jadhav, K.K.K. Sharma, N.R. Prasad, Bos taurus (A-2) urine assisted bioactive cobalt oxide anchored ZnO: a novel nanoscale approach, Sci. Rep. 12 (1) (2022) 15584.
[50] S. Kumar, G. Kaur, M. Rawat, Y.F. Tsang, K.-Y. Lin, K.-H. Kim, Potential of Piper betle@Co3O4 nanoparticles as high-performance photocatalysts for the removal of industrial dyes, J. Cleaner Prod. 361 (2022) 132242.
[51] M.M. Margoni, G. Rajivgandhi, C. Gnanasekaran, C.K. Chelliah, S. Sathik Basha, G. Ramachandran, M. Maruthupandy, M. Dhanasekar, F. Quero, A. Akbari-Fakhrabadi, V.R. Bhaviripudi, S. Kadaikunnan, T.N. Almanaa, Eco-friendly synthesis of Co3O4 nanoparticles using Millettia pinnata towards increased anti-oxidant, anti-biofilm and cytocompatibility properties against biofilm producing bacteria and human pulmonary alveolar basal cells, J. Drug Deliv. Sci. Technol. 100 (2024) 106124.
[52] S. Kavica, P. Rajesh, V. Velmani, G. Parethe, Biological synthesis of cobalt oxide nanoparticles using Ziziphus oenopolia leaf extract, J. Environ. Nanotechnol 13 (1) (2024) 85–91.
[53] S.Z. Mohammadi, B. Lashkari, A. Khosravan, Green synthesis of Co3O4 nanoparticles by using walnut green skin extract as a reducing agent by using response surface methodology, Surf. Interfaces. 23 (2021) 100970.
[54] S. Drummer, O. Mkhari, M. Chowdhury, Green synthesis of Co3O4 nanoparticles using spent coffee: application in catalytic and photocatalytic dye degradation, Next Nanotechnol. 6 (2024) 100069.
[55] S. Batool, M. Hasan, M. Dilshad, A. Zafar, T. Tariq, Z. Wu, R. Chen, S. Gul Hassan, T. Munawar, F. Iqbal, M. Saqib Saif, M. Waqas, X. Shu, Green synthesis of cordia myxa incubated ZnO, Fe2O3, and Co3O4 nanoparticle: characterization, and their response as biological and photocatalytic agent, Adv. Powder Technol. 33 (11) (2022) 103780.
[56] R. Zimmermann, P. Steiner, R. Claessen, F. Reinert, S. Hüfner, P. Blaha, P. Dufek, Electronic structure of 3d-transition-metal oxides: on-site Coulomb repulsion versus covalency, J. Phys.: Condens. Matter 11 (7) (1999) 1657.
[57] B.R. Alsehli, F.M. Alminderej, M.H.A. Hassan, M.F. Al-Hakkani, S.M. Saleh, D. S. Mohamed, Biosynthesis, characterizations, and comparison of TiO2/CeO2/their nanocomposites as bio-adsorbents of linezolid and their microbiological activities, J. Mol. Struct. 1328 (2025) 141388.
[58] B.R. Alsehli, M.F. Al-Hakkani, A.H. Alluhayb, S.M. Saleh, H. Mohamed, A.M. A. Hassane, M.H.A. Hassan, Facile mycosynthesis of selenium nanoparticles by Aspergillus candidus extract: unveiling characterization, potent antimicrobial properties, and cytotoxic activities, J. Bionanosci. 15 (2) (2025) 234.
[59] B.R. Alsehli, M.F. Al-Hakkani, A.H. Alluhayb, S.M. Saleh, M.M.M. Abdelrahem, A. M.A. Hassane, M.H.A. Hassan, Sustainable Myco-synthesis of antimony oxide nanoparticles using endophytic penicillium chrysogenum Extract: characterization, antimicrobial potency, and cytotoxicity assays, Inorg. Chem. Commun. 173 (2025) 113793.
[60] S. Savitha, S. Surendhiran, T.M.N. Vidaarth, K.S.G. Jagan, A. Karthik, R. Sabarirajan, Evaluation of physiochemical and in-vitro characteristics of Ixora Coccinea mediated Co3O4 nanoparticles for photocatalytic degradation of toxic textile dye effluents, J. Indian Chem. Society 101 (10) (2024) 101352.
[61] R. Govindasamy, V. Raja, S. Singh, M. Govindarasu, S. Sabura, K. Rekha, V. D. Rajeswari, S.S. Alharthi, M. Vaiyapuri, R. Sudarmani, S. Jesurani, B. Venkidasamy, M. Thiruvengadam, Green synthesis and characterization of cobalt oxide nanoparticles using psidium guajava leaves extracts and their photocatalytic and biological activities, Molecules. 27 (17) (2022) 5646.